

Quantum Crosstalk Robust Quantum Control

Zeyuan Zhou,¹ Ryan Sitler,² Yasuo Oda,¹ Kevin Schultz,² and Gregory Quiroz^{2,1}

¹William H. Miller III Department of Physics & Astronomy,
Johns Hopkins University, Baltimore, Maryland 21218, USA

²Johns Hopkins University Applied Physics Laboratory

The prevalence of quantum crosstalk in current quantum devices poses challenges for achieving high-fidelity quantum logic operations and reliable quantum processing. Through quantum control theory, we develop an analytical condition for achieving crosstalk-robust single-qubit control of multi-qubit systems. We examine the effects of quantum crosstalk via a cumulant expansion and develop a condition to suppress the leading order contributions to the dynamics. The efficacy of the condition is illustrated in the domains of quantum state preservation and noise characterization through the development of crosstalk-robust dynamical decoupling and quantum noise spectroscopy (QNS) protocols. Using the IBM Quantum Experience, crosstalk-robust state preservation is demonstrated on 27 qubits, where a 3× improvement in coherence decay is observed for single-qubit product and multipartite entangled states. Through the use of noise injection, we experimentally demonstrate crosstalk-robust dephasing QNS on a seven qubit processor, where a 10⁴ improvement in reconstruction accuracy over “cross-susceptible” alternatives is found. Together, these experiments highlight the significant impact the crosstalk mitigation condition can have on improving multi-qubit characterization and control on current quantum devices.

The ability to implement high-fidelity quantum logic operations is a necessity for achieving reliable and scalable quantum computing [1]. In current systems, however, system-environment interaction and crosstalk are typically quite substantial and ultimately limit qubit coherence and gate accuracies. Characterized as unwanted inter-qubit coupling, quantum crosstalk causes undesired dynamics that violate the locality and individual addressability of qubits. It is known to be prevalent in current systems and present obstacles in the implementation of quantum algorithms [2–6], quantum characterization [7–10], and instantiations of quantum error correction [11, 12].

Quantum crosstalk arises in a variety of qubit architectures. Atomic systems are susceptible to unwanted interactions between neighboring spectator qubits during two-qubit operations [12–17], while superconductor (e.g., fixed-frequency transmons [18–21]) and semiconductor [22–24] platforms commonly experience parasitic ZZ interactions from always-on coupling used to implement entangling gates. Various strategies have been proposed to address crosstalk from the hardware and software perspective. Hardware solutions have predominately centered around architecture design [25–27]. Software approaches are diverse and have sought to address crosstalk at the physical [6, 17, 22, 28–30] and compiler [2, 3, 31, 32] layers of the quantum software stack. Despite their utility, these approaches are either hardware-specific or provide limited insight and intuition into broader principles for crosstalk mitigation.

We address this challenge by leveraging quantum control theory to develop an analytical condition for achieving crosstalk robust single-qubit control of multi-qubit systems. Quantum control is a widely used tool for constructing high-fidelity gates [33–38] and error mitigation strategies [39–42], as well as unraveling key characteristics of spatio-temporally correlated noise through quantum noise spectroscopy (QNS) [43–52]. We exploit a control frame-

work commonly used to derive the filter function formalism [34, 35, 47, 53–55] to examine the impact of crosstalk on system dynamics. Through the use of a perturbative cumulant-based expansion, we derive a control condition that enables quantum crosstalk cancellation up to second order in the total evolution time.

The versatility and applicability of our approach is illustrated through experimental investigations of crosstalk robust quantum state preservation and noise characterization on the IBM Quantum Experience (IBMQE). Crosstalk-robust dynamical decoupling (CRDD) is introduced and shown to dramatically improve the simultaneous preservation of single-qubit product states (SPSs) and multipartite entangled states (MESs) up to 27 qubits. Furthermore, we demonstrate the relevance of the condition to noise characterization, where a crosstalk-robust dephasing QNS protocol is introduced and subsequently used to perform the first known simultaneous noise spectrum estimation on seven qubits. Together, these experiments highlight the deleterious effects of crosstalk and the remarkable impact our condition can have on improving multi-qubit characterization and control on current quantum devices.

Crosstalk Noise Model. – We focus on the suppression of crosstalk during the implementation of single qubit operations as this represents the most fundamental type of control one may possess on a quantum system. To this end, we consider an N qubit system subject to noisy, controlled evolution governed by the time-dependent Hamiltonian $H(t) = H_C(t) + H_E(t)$. The control Hamiltonian is given by

$$H_C(t) = \sum_{i=1}^N \frac{\Omega_i(t)}{2} (\sigma_i^x \cos \phi_i(t) + \sigma_i^y \sin \phi_i(t)), \quad (1)$$

where $\Omega_i(t)$ and $\phi_i(t)$ represent the time-dependent control amplitude and phase, respectively. Noise is generated by the

error Hamiltonian

$$H_E(t) = \sum_{i=1}^N \vec{\sigma}_i \cdot \vec{\beta}_i(t) + \sum_{i<j}^N J_{ij} \sigma_i^z \sigma_j^z, \quad (2)$$

with $\vec{\sigma}_i = (\sigma_i^x, \sigma_i^y, \sigma_i^z)$ consisting of the i th qubit Pauli operators. All relevant noise contributions are captured by semi-classical, spatio-temporally correlated noise processes and static quantum crosstalk. The former is described by $\vec{\beta}_i(t) = (\beta_i^x(t), \beta_i^y(t), \beta_i^z(t))$, where $\beta_i^\mu(t)$ is assumed to be a wide-sense stationary Gaussian stochastic process with zero-mean, $\overline{\beta_i^\mu(t)} = 0$, and two-point correlation functions $C_{ij}^{\mu\nu}(\tau) = \overline{\beta_i^\mu(\tau)\beta_j^\nu(0)}$, $\mu, \nu = x, y, z$. Note that $\overline{\quad}$ denotes classical ensemble averaging. The crosstalk is characterized by the static coupling strength J_{ij} and 2-local ZZ interactions. This model and its generalization [56] are relevant to a wide range of experimental platforms, including superconducting qubits [18, 19, 26, 44], semiconductor qubits [22, 23, 52, 57], and trapped ion systems [12, 13, 17, 48, 50, 58].

Effective Error Dynamics. – We investigate the effect of $H_E(t)$ on the dynamics of expectation values and fidelity using time-dependent perturbation theory. In the limit of strong control and weak noise [47, 55, 59], the dynamics are dominated by the control such that $H_E(t)$ is treated as a perturbation. The evolution generated by the error Hamiltonian is isolated by moving into the interaction (togglng) frame with respect to the control such that the total evolution is described by $U(T) = \tilde{U}_E(T)U_C(T)$. The propagator $U_C(T) = U_C(T, 0) = \mathcal{T}_+ e^{-i \int_0^T dt H_C(t)}$ describes the control dynamics, while $\tilde{U}_E(T) = \mathcal{T}_+ e^{-i \int_0^T dt \tilde{H}_E(t)}$ is the rotated-frame time evolution governed by $\tilde{H}_E(t) = U_C(T, t)H_E(t)U_C^\dagger(T, t)$; \mathcal{T}_+ denotes the time-ordering operator. The rotated-frame error Hamiltonian is further specified by

$$\tilde{H}_E(t) = \sum_{i=1}^N \tilde{\Lambda}_i(t) \cdot \vec{\beta}_i(t) + \sum_{i,j=1}^N J_{ij} [\tilde{\Lambda}_i^T(t)]_z [\tilde{\Lambda}_j(t)]_z, \quad (3)$$

where $\tilde{\Lambda}_i(t) \equiv \mathbf{R}_i(t)\vec{\sigma}_i^T$ and $\mathbf{R}_i(t)$ is the ‘‘control matrix’’ with elements $R_i^{\mu\nu}(t) = \text{Tr}[U_C(T, t)\sigma_i^\mu U_C^\dagger(T, t)\sigma_i^\nu]/2$. A^T and $[\vec{a}]_z$ denote the transpose of A and the z -component of \vec{a} , respectively.

We quantify the impact of noise on the time-dependent expectation value of an observable O using a cumulant based perturbative expansion. In the weak noise limit, the noise-averaged expectation value $\overline{\langle O(T) \rangle} = \overline{\text{Tr}[\rho(T)O]}$ with respect to the time-evolved state $\rho(T) = U(T)\rho(0)U^\dagger(T)$ can be approximated as

$$\overline{\langle O(T) \rangle} \approx \text{Tr}[e^{-iC_O^{(1)}(T)+C_O^{(2)}(T)/2} \rho_C(T)O]. \quad (4)$$

$\rho_C(T) = U_C(T)\rho(0)U_C^\dagger(T)$ represents the time-evolved state with respect to the ideal control dynamics [47, 59], while the error dynamics generated by $H_E(t)$ are described by the

first and second cumulants:

$$C_O^{(1)}(T) = \sum_{i<j}^N \sum_{\mu, \nu=x,y,z} \chi_{ij}^{\mu\nu}(T) (\sigma_i^\mu \sigma_j^\nu - O^{-1} \sigma_i^\mu \sigma_j^\nu O) \quad (5)$$

$$C_O^{(2)}(T) = \sum_{i,j=1}^N \sum_{\nu, \gamma=x,y,z} \Gamma_{ij}^{\nu\gamma}(T) \mathcal{A}_{ij}^{\nu\gamma}, \quad (6)$$

The cumulants are determined by the operator $\mathcal{A}_{ij}^{\nu\gamma} = \sigma_i^\nu \sigma_j^\gamma + O^{-1} \sigma_i^\nu \sigma_j^\gamma O - O^{-1} \sigma_i^\nu O \sigma_j^\gamma - \sigma_i^\nu O^{-1} \sigma_j^\gamma O$ and the overlap integrals

$$\chi_{ij}^{\mu\nu}(T) \equiv J_{ij} \int_0^T R_i^{z\mu}(t) R_j^{z\nu}(t) dt, \quad (7)$$

$$\Gamma_{ij}^{\nu\gamma}(T) \equiv \sum_{\mu, \delta=x,y,z} \int_0^\infty \frac{d\omega}{2\pi} \mathcal{G}_{ij}^{\mu\nu\delta\gamma}(\omega, T) S_{ij}^{\mu\delta}(\omega), \quad (8)$$

with $S_{ij}^{\mu\nu}(\omega) = \int_0^T C_{ij}^{\mu\nu}(\tau) e^{-i\omega\tau} dt$ designating the noise power spectral density. The filter functions $\mathcal{G}_{ij}^{\mu\nu\delta\gamma}(\omega, T) \equiv \text{Re}[G_i^{\mu\nu}(\omega, T)G_j^{\delta\gamma}(-\omega, T)]$ are defined in terms of the Fourier transforms of the elements of the control matrix: $G_i^{\mu\nu}(\omega, T) \equiv \int_0^T R_i^{\mu\nu}(t) e^{i\omega t} dt$. Note that the first cumulant is solely composed of crosstalk contributions, while the second cumulant only contains system-environment interactions.

Similar expressions can be obtained for the fidelity (i.e., overlap) between the initial state $\rho(0)$ and time-evolved state $\rho(T)$. When $\rho(0)$ is a pure state, the noise-averaged fidelity is given by $\mathcal{F}(T) = \text{Tr}[\rho(T)\rho(0)]$. In general, $\rho(0)$ can be non-invertible which poses challenges for recasting $\mathcal{F}(T)$ in the form of Eq. (4) [56]. However, by expanding the initial state as a sum of invertible, Hermitian operators: $\rho(0) = \sum_\ell \Phi_\ell$, the fidelity can be approximated as

$$\mathcal{F}(T) \approx \sum_\ell \text{Tr}[e^{-iC_{\Phi_\ell}^{(1)}(T)+C_{\Phi_\ell}^{(2)}(T)/2} \rho_C(T)\Phi_\ell]. \quad (9)$$

The expansion of $\rho(0)$ is particularly applicable for qubit systems, where Φ_i may be chosen to be proportional to the N -qubit Pauli operators. While the cumulant expressions of Eq. (9) differ from those of Eq. (4) in the operator conjugations, their commonality lies in the overlap integrals $\chi_{ij}^{\mu\nu}(T)$ and $\Gamma_{ij}^{\nu\gamma}(T)$. These quantities are exclusively dependent upon the specifications of the noise model and the control.

Crosstalk-Robust Control Condition. – In the cumulant representation, a control protocol defined by $\{\Omega_i(t), \phi_i(t)\}_{i=1}^N$ attains n th order suppression of the error dynamics when $C_O^{(k)}(T) = 0$ for $k \leq n$. Suppression of the first cumulant is achieved by cancellation of the pure crosstalk contribution, or more specifically, satisfying the *crosstalk suppression condition*:

$$\chi_{ij}^{\mu\nu}(T) = 0 \quad \forall i, j, \mu, \nu. \quad (10)$$

Due to the static nature of J_{ij} , $C_O^{(2)}(T)$ is completely dominated by system-environment interactions. As such, imposing Eq. (10) in conjunction with minimizing the spectral overlap

between the system-environment noise and the filter functions leads to second order suppression of all noise contributions.

The efficacy of the above condition is explored in the next sections via experimental realizations of quantum state preservation and QNS on the IBMQE. Composed of fixed-frequency transmons, IBMQE processors are susceptible to parasitic ZZ -crosstalk [7, 19, 30] and temporally-correlated noise [30, 60–63], both of which are captured by Eq. (2). Thus, they present suitable testbeds for evaluating and showcasing the potential impact of imposing Eq. (10).

Quantum State Preservation – We demonstrate the utility of the above condition in the context of quantum state preservation through the design and experimental evaluation of CRDD. DD selectively averages out unwanted interactions between a quantum system and its environment and combats systematic errors through the use of fast and strong pulses [41]. When properly designed, DD preserves the state of a single qubit system, while suppressing static quantum crosstalk [30]. Here, we show how the above condition enables greater generality for simultaneous preservation of an array of qubits initialized in SPSs and MESSs.

While the crosstalk suppression condition allows for a diverse family of possible CRDD protocols, for concreteness, we focus on those inspired by XY4 [39]. This sequence utilizes repetitions of $f_\tau X f_\tau Y f_\tau X f_\tau Y$, where X and Y are π -pulses (of duration δ) about the x and y axis of the single qubit Bloch sphere, respectively. Free evolution periods f_τ , where the system evolves according to its internal dynamics, are of duration τ ; thus, yielding a cycle time of $t_{XY4} = 4(\tau + \delta)$. XY4 affords suppression of system-environment interactions to first order in time-dependent perturbation theory [39].

Crosstalk-robust state preservation is achieved by properly adjusting the pulse locations of multi-qubit variants of XY4.

Given an array of qubits, the suppression condition is enforced by patterning two sequences across the array: XY4 and $XY4' = X f_\tau Y f_\tau X f_\tau Y f_\tau$; this protocol is labeled CR-XY4. An example of the protocol is shown in the inset of Fig. 1(a). In the ideal, instantaneous pulse limit, simultaneous application of these sequences results in universal single qubit decoupling and proper tailoring of the control matrix to suppress crosstalk. In the DD context, the suppression condition is equivalent to enforcing the typical anti-commutativity required to achieve first-order decoupling [41]. As such, variants of CRDD based on time-symmetric XY4 [64] and Eulerian DD [65] may be considered as well.

CR-XY4 is experimentally evaluated against free evolution and XY4. The three protocols are compared by simultaneously preparing N qubits in the state $|\Psi\rangle = \otimes_{i=1}^N |\psi_i\rangle$, where $|\psi_i\rangle$ is a state in the xy -plane of the single-qubit Bloch sphere. Then, M repetitions (or the free evolution equivalent) of the protocol are applied for a total time $T = Mt_{XY4} = Mt_{CR-XY4}$. For all devices discussed below, $\tau = \delta = 35$ ns. The experiment is completed by applying the inverse state preparation unitary followed by a measurement in the computational basis. Resulting measurements are used to estimate the fidelity $\mathcal{F}(T)$ between $\rho(0) = |\Psi\rangle\langle\Psi|$ and $\rho(T)$ resulting from free

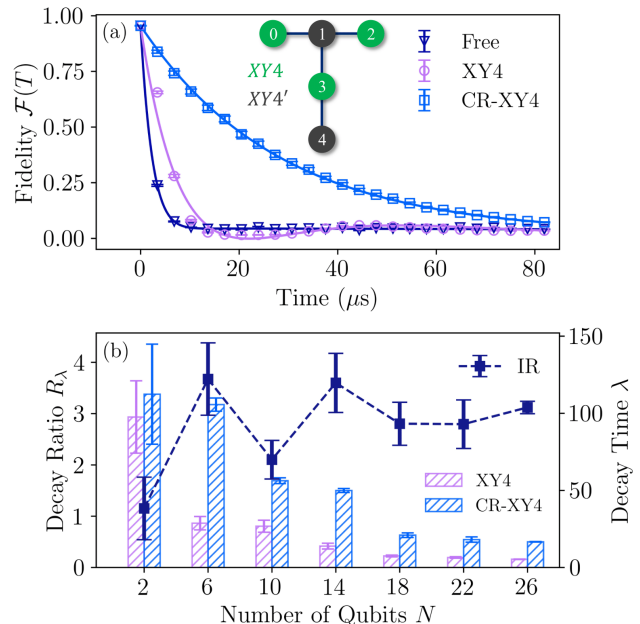


FIG. 1. Simultaneous preservation of SPSs using different control protocols. (a) Fidelity vs. time for the IBMQE Lima 5-qubit processor using free evolution (dark blue down-triangles), XY4 (light purple circles), and CR-XY4 (light blue squares). Data points and error bars denote mean fidelity and CIs, respectively, obtained from bootstrapping. Inset: CR-XY4 protocol on IBMQE Lima; similar patterning used for IBMQE Auckland. (b) Fidelity decay rate comparison between XY4 and CR-XY4 using up to 26 qubits on IBMQE Auckland. Bars represent mean decay time λ (with CI error bars), while the line signifies the IR. Results are collected using the same procedure outlined for the top panel. In both cases, CR-XY4 exhibits significant improvement over XY4.

or DD evolution. We focus on states in the xy -plane as these are among the most susceptible to ZZ -crosstalk.

CR-XY4 substantially improves the fidelity of SPSs. In Fig. 1(a), a comparison between the protocols is shown for the IBMQE Lima 5-qubit processor. Estimates of average fidelity and 95% confidence intervals (CIs) are determined via bootstrapping (with replacement) [66] from 1000 resamples of data collected from 20 random qubit states in the xy -plane, 8000 shots, and four replicates of the experiment run over four days. The data is fit to the modified exponential decay [42]: $F(t) = c[1 - f(t)] + F_0$, where $f(t) = 1/(1+k)(ke^{-t/\lambda} \cos(t\gamma) + e^{-t/\alpha})$, and $c = (F_{T_{\max}} - F_0)/(f(T_{\max}) - 1)$. The model includes short and long decay times λ and α , respectively, oscillation frequency γ , and dimensionless weight parameter k . The calculated fidelity at $M = 0$ and $M = M_{\max}$ are given by F_0 and $F_{T_{\max}}$, respectively. A comparison of the short decay times via the ratio $R_\lambda = \lambda_{CR-XY4}/\lambda_{XY4}$ reveals a factor of 4 improvement for CR-XY4 over XY4. While the enhancement varies as the number of qubits increases due to hardware variability, it remains near a $3\times$ improvement up to 26 qubits, as shown experimentally on IBMQE Auckland in Fig. 1(b).

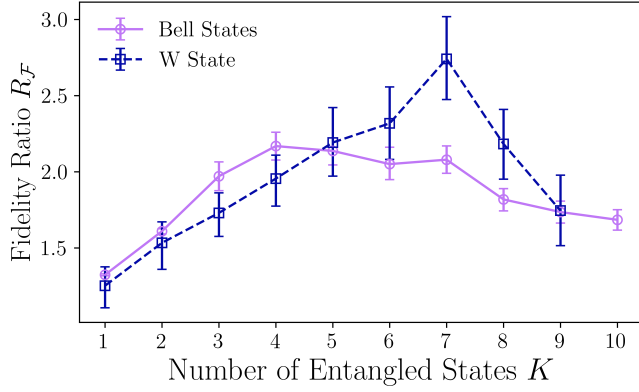


FIG. 2. Ratio of time-averaged fidelities of CR-XY4 and XY4 for the simultaneous protection of K MESs on the 27-qubit IBMQE Auckland processor. Plot contains results for Bell states (light purple circles) and the W state (dark blue squares). Bell state results are collected using 8000 shots, the four Bell states, and five replicates of the experiment collected over five days. Similar data is collected for the W state. Averages and CIs are determined by bootstrapping, where 1000 resamples of the data are used. Results indicate that CR-XY4 improves state preservation over XY4 for both cases.

CR-XY4 considerably enhances the time-average fidelity of MESs. In Fig. 2, N qubits are simultaneously prepared in K' entangled states and then subject to M repetitions of XY4 or CR-XY4. Then, prior to measurement in the computational basis, the inverse state preparation unitary is applied. Upon applying up to $M_{\max} = 50$ repetitions of DD, the time-averaged fidelity $\mathcal{F}_{\text{avg}} = T_{\max}^{-1} \int_0^{T_{\max}} \frac{\mathcal{F}(t)}{\mathcal{F}(0)} dt$ is calculated via numerical integration for each DD protocol [67]. Note that this measure captures long-time behavior, with the normalization accounting for state preparation errors. In Fig. 2, \mathcal{F}_{avg} is conditioned on the simultaneous preservation of $K \leq K'$ states on physically adjacent qubits. We consider $N = 20$ qubits simultaneously prepared in $K' = 10$ Bell states of the form $|\Phi_{\pm}\rangle = 1/\sqrt{2}(|00\rangle \pm |11\rangle)$ or $|\Psi_{\pm}\rangle = 1/\sqrt{2}(|01\rangle \pm |10\rangle)$. A similar procedure is used for the three-qubit W state $|W\rangle = 1/\sqrt{3}(|001\rangle + |010\rangle + |100\rangle)$, where $K' = 9$ entangled states are prepared on $N = 27$ qubits. In Fig. 2, the fidelity ratio $R_{\mathcal{F}} = \mathcal{F}_{\text{avg}}^{\text{CR-XY4}}/\mathcal{F}_{\text{avg}}^{\text{XY4}}$ is shown for both state preparations. \mathcal{F}_{avg} collected from all initial states, 8000 shots, and five replicates of the experiments are used to estimate $R_{\mathcal{F}}$ and CIs via bootstrapping [56]. Individual Bell states are invariant under ZZ -crosstalk, however, multiple Bell states prepared physically adjacent on the quantum device experience ZZ -crosstalk across the common edge. The impact of suppressing edge effects is observed via the $2\times$ improvement over XY4 obtained by CR-XY4. The W state does not possess inherent robustness and therefore experiences a greater benefit from CRDD; a near $3\times$ improvement. Despite the increasing contributions from state preparation and measurement and gate error observed at large N , CR-XY4 continues to achieve a slower decay in fidelity than XY4 and hence, a higher time-averaged fidelity for both MES preparations considered.

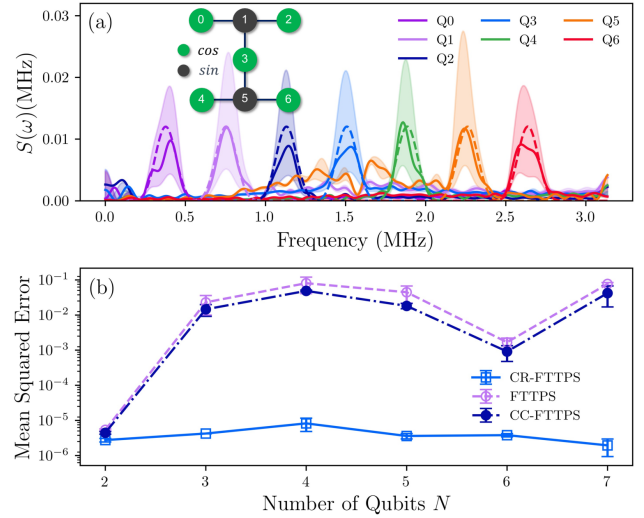


FIG. 3. Crosstalk-robust QNS on the 7-qubit IBMQE Nairobi processor, where narrowband dephasing noise with distinct center frequencies is injected on each qubit. (a) Seven-qubit simultaneous local dephasing QNS using CR-FTTPS. Average spectrum estimates (solid lines) and CIs (shaded regions) indicate good agreement with injected noise (dashed lines). Inset: CR-FTTPS protocol on Nairobi. (b) Reconstruction error as a function of the number of qubits for FTTMS variants. Data points denote averages and error bars are CIs. CR-FTTMS outperforms other variants considered by up to 4 orders of magnitude. Averages and CIs are determined from bootstrapping.

Quantum Noise Spectroscopy – The crosstalk suppression condition can inform the design of QNS protocols. In QNS, a controlled quantum system is used as a dynamical probe to characterize the spectral properties of environmental noise. Under the zero-mean noise assumption, spectrum estimates are determined by tailoring the frequency response of the system via control, estimating expectation value decay rates, and using $\mathcal{C}_O^{(2)}(T)$ to define a linear inversion problem at discrete frequencies [43, 44]. Crosstalk introduces spurious features in spectral estimates that are further exacerbated by imperfections in the control [56]. We construct pulse-based sequences that provide robustness to both crosstalk and errors due to finite pulse duration while enabling estimates of local dephasing noise spectra on a collection of qubits.

In particular, we design a crosstalk-robust variant of the Fixed Total Time Pulse Sequences (FTTMS) [68, 69]. Book-ended by two $X_{\pi/2}$ pulses, FTTMS consist of $\ell/2$ different sequences, each containing ℓ gates. In the instantaneous pulse limit, “cosine” FTTMS yield the discrete-time control matrix $R_i^{zz}(t) = \text{sgn}\{\cos(\pi(\kappa-1)m/\ell)\}$ for $\kappa, m = 1, \dots, \ell/2$. Sign changes in the cosine function denote locations of X gates and I gates otherwise. Simultaneous application of “cosine” FTTMS on multiple qubits preserves the first cumulant and therefore crosstalk. However, by introducing an additional “sine” FTTMS described by $R_i^{zz}(t) = \text{sgn}\{\sin(\pi(\kappa-1)m/\ell)\}$ alternating the qubit array with the cosine and sine variants, one can effectively implement crosstalk-robust FTTMS (CR-

FTTPS).

Using the IBMQE Nairobi 7-qubit processor, we inject narrow band dephasing noise at N distinct frequencies on N qubits via the Schrodinger Wave Moving Average Model (SchWARMA) approach [69]. The spectrum reconstruction accuracy of CR-FTTPS and FTTPS for $\ell = 128$ is assessed using 10 SchWARMA trajectories and five data sets collected over five days. Bootstrapped spectrum estimates and CIs are determined from 1000 resamples of the reconstructed spectra. Figure 3(a) shows spectrum estimates using CR-FTTPS on 7 qubits, where average spectrum estimates (solid lines) and CIs (shaded regions) agree well with the injected spectra (dotted lines). Analyzing the mean-squared error between estimated and injected spectra as a function of the number of qubits [Fig. 3(b)], we find that CR-FTTPS achieves a 10^4 improvement over FTTPS in reconstruction accuracy. This enhancement is due to suppression of ZZ , as well as pulse-error-induced ZY and YZ -crosstalk. We substantiate this claim empirically by considering crosstalk-corrected FTTPS (CC-FTTPS), where ZZ -crosstalk is included in the spectrum reconstruction by using IBM-measured crosstalk coupling strengths; only slight improvements are observed. CR-FTTPS robustness is further justified analytically in the supplement.

Conclusions – Through the lens of quantum control, we develop a condition for first-order quantum crosstalk suppression for general single qubit control of multi-qubit systems. The utility of the condition is demonstrated in the domains of quantum state preservation and noise characterization, where we design crosstalk robust DD and QNS, respectively. Through experimental investigations on the IBMQE, we showcase the significance of the condition in each domain on various processors, simultaneously mitigating crosstalk on up to 27 qubits. Together, these experiments highlight the crucial impact our condition can have on improving simultaneous characterization and control on current quantum devices.

Acknowledgements – This work was supported by the U.S. Department of Energy, Office of Science, Office of Advanced Scientific Computing Research, Accelerated Research in Quantum Computing under Award Number DE-SC0020316. KS and GQ acknowledge support from ARO MURI grant W911NF-18-1-0218. This research used resources of the Oak Ridge Leadership Computing Facility, which is a DOE Office of Science User Facility supported under Contract DE-AC05-00OR22725.

[1] J. Preskill, *Quantum* **2**, 79 (2018).

[2] Y. Ding, P. Gokhale, S. F. Lin, R. Rines, T. Propson, and F. T. Chong, in *2020 53rd Annual IEEE/ACM International Symposium on Microarchitecture (MICRO)* (IEEE, 2020).

[3] P. Murali, D. C. McKay, M. Martonosi, and A. Javadi-Abhari, in *Proceedings of the Twenty-Fifth International Conference on Architectural Support for Programming Languages and Operating Systems* (ACM, 2020).

- [4] D. V. Babukhin and W. V. Pogosov, *Quantum Information Processing* **21** (2021), 10.1007/s11128-021-03346-z.
- [5] Y. Ohkura, T. Satoh, and R. Van Meter, *IEEE Transactions on Quantum Engineering* **3**, 1 (2022).
- [6] L. Xie, J. Zhai, Z. Zhang, J. Allcock, S. Zhang, and Y.-C. Zheng, in *Proceedings of the 27th ACM International Conference on Architectural Support for Programming Languages and Operating Systems* (ACM, 2022).
- [7] J. M. Gambetta, A. D. Córcoles, S. T. Merkel, B. R. Johnson, J. A. Smolin, J. M. Chow, C. A. Ryan, C. Rigetti, S. Poletto, T. A. Ohki, M. B. Ketchen, and M. Steffen, *Physical Review Letters* **109** (2012), 10.1103/physrevlett.109.240504.
- [8] D. C. McKay, S. Sheldon, J. A. Smolin, J. M. Chow, and J. M. Gambetta, *Phys. Rev. Lett.* **122**, 200502 (2019).
- [9] M. Sarovar, T. Proctor, K. Rudinger, K. Young, E. Nielsen, and R. Blume-Kohout, *Quantum* **4**, 321 (2020).
- [10] K. Rudinger, C. W. Hogle, R. K. Naik, A. Hashim, D. Lobser, D. I. Santiago, M. D. Grace, E. Nielsen, T. Proctor, S. Seritan, S. M. Clark, R. Blume-Kohout, I. Siddiqi, and K. C. Young, *PRX Quantum* **2**, 040338 (2021).
- [11] Z. Chen, K. J. Satzinger, J. Atalaya, A. N. Korotkov, A. Dunsworth, D. Sank, C. Quintana, M. McEwen, R. Barends, P. V. Klimov, *et al.*, [arXiv:2102.06132](https://arxiv.org/abs/2102.06132) (2021).
- [12] P. Parrado-Rodríguez, C. Ryan-Anderson, A. Bermudez, and M. Müller, *Quantum* **5**, 487 (2021).
- [13] C. Ospelkaus, C. E. Langer, J. M. Amini, K. R. Brown, D. Leibfried, and D. J. Wineland, *Physical review letters* **101**, 090502 (2008).
- [14] E. Urban, T. A. Johnson, T. Henage, L. Isenhower, D. Yavuz, T. Walker, and M. Saffman, *Nature Physics* **5**, 110 (2009).
- [15] J. M. Auger, S. Bergamini, and D. E. Browne, *Phys. Rev. A* **96**, 052320 (2017).
- [16] H. Levine, A. Keesling, A. Omran, H. Bernien, S. Schwartz, A. S. Zibrov, M. Endres, M. Greiner, V. Vuletić, and M. D. Lukin, *Phys. Rev. Lett.* **121**, 123603 (2018).
- [17] C. Fang, Y. Wang, S. Huang, K. R. Brown, and J. Kim, [arXiv:2206.02703](https://arxiv.org/abs/2206.02703) (2022).
- [18] P. Krantz, M. Kjaergaard, F. Yan, T. P. Orlando, S. Gustavsson, and W. D. Oliver, *Applied Physics Reviews* **6**, 021318 (2019).
- [19] A. Ash-Saki, M. Alam, and S. Ghosh, *IEEE Transactions on Quantum Engineering* **1**, 1 (2020).
- [20] A. Kandala, K. X. Wei, S. Srinivasan, E. Magesan, S. Carnevale, G. A. Keefe, D. Klaus, O. Dial, and D. C. McKay, *Phys. Rev. Lett.* **127**, 130501 (2021).
- [21] P. Zhao, K. Linghu, Z. Li, P. Xu, R. Wang, G. Xue, Y. Jin, and H. Yu, *PRX Quantum* **3**, 020301 (2022).
- [22] D. Buterakos, R. E. Throckmorton, and S. D. Sarma, *Physical Review B* **97** (2018), 10.1103/physrevb.97.045431.
- [23] I. Heinz and G. Burkard, *Phys. Rev. B* **105**, 085414 (2022).
- [24] R. E. Throckmorton and S. Das Sarma, *Phys. Rev. B* **105**, 245413 (2022).
- [25] P. Mundada, G. Zhang, T. Hazard, and A. Houck, *Physical Review Applied* **12** (2019).
- [26] J. Ku, X. Xu, M. Brink, D. C. McKay, J. B. Hertzberg, M. H. Ansari, and B. L. T. Plourde, *Phys. Rev. Lett.* **125**, 200504 (2020).
- [27] P. Zhao, P. Xu, D. Lan, J. Chu, X. Tan, H. Yu, and Y. Yu, *Phys. Rev. Lett.* **125**, 200503 (2020).
- [28] A. R. R. Carvalho, H. Ball, M. J. Biercuk, M. R. Hush, and F. Thomsen, *Phys. Rev. Applied* **15**, 064054 (2021).
- [29] K. Wei, E. Magesan, I. Lauer, S. Srinivasan, D. Bogorin, S. Carnevale, G. Keefe, Y. Kim, D. Klaus, W. Landers, *et al.*, [arXiv:2106.00675](https://arxiv.org/abs/2106.00675) (2021).
- [30] V. Tripathi, H. Chen, M. Khezri, K.-W. Yip, E. M. Levenson-

- Falk, and D. A. Lidar, (2021), [10.48550/ARXIV.2108.04530](https://arxiv.org/abs/2010.04530).
- [31] C. Zhang, Y. Chen, Y. Jin, W. Ahn, Y. Zhang, and E. Z. Zhang, [arXiv:2009.02346](https://arxiv.org/abs/2009.02346) (2020).
- [32] B. Zhang, S. Majumder, P. H. Leung, S. Crain, Y. Wang, C. Fang, D. M. Debroy, J. Kim, and K. R. Brown, *Physical Review Applied* **17** (2022), [10.1103/physrevapplied.17.034074](https://doi.org/10.1103/physrevapplied.17.034074).
- [33] D. Dong and I. R. Petersen, *IET control theory & applications* **4**, 2651 (2010).
- [34] T. J. Green, J. Sastrawan, H. Uys, and M. J. Biercuk, *New Journal of Physics* **15**, 095004 (2013).
- [35] H. Ball and M. J. Biercuk, *EPJ Quantum Technology* **2**, 1 (2015).
- [36] F. K. Wilhelm, S. Kirchhoff, S. Machnes, N. Wittler, and D. Sugny, arXiv preprint [arXiv:2003.10132](https://arxiv.org/abs/2003.10132) (2020).
- [37] D. d'Alessandro, *Introduction to quantum control and dynamics* (Chapman and hall/CRC, 2021).
- [38] Y. Oda, D. Lucarelli, K. Schultz, B. D. Clader, and G. Quiroz, (2022).
- [39] L. Viola, E. Knill, and S. Lloyd, *Phys. Rev. Lett.* **82**, 2417 (1999).
- [40] M. Biercuk, A. Doherty, and H. Uys, *Journal of Physics B: Atomic, Molecular and Optical Physics* **44**, 154002 (2011).
- [41] *Quantum Error Correction* (Cambridge University Press, 2013).
- [42] B. Pokharel, N. Anand, B. Fortman, and D. A. Lidar, *Phys. Rev. Lett.* **121**, 220502 (2018).
- [43] G. A. Álvarez and D. Suter, *Phys. Rev. Lett.* **107**, 230501 (2011).
- [44] J. Bylander, S. Gustavsson, F. Yan, F. Yoshihara, K. Harrabi, G. Fitch, D. G. Cory, Y. Nakamura, J.-S. Tsai, and W. D. Oliver, *Nature Physics* **7**, 565 (2011).
- [45] L. Cywiński, *Phys. Rev. A* **90**, 042307 (2014).
- [46] L. M. Norris, G. A. Paz-Silva, and L. Viola, *Phys. Rev. Lett.* **116**, 150503 (2016).
- [47] G. A. Paz-Silva, L. M. Norris, and L. Viola, *Phys. Rev. A* **95**, 022121 (2017).
- [48] V. Frey, S. Mavadia, L. Norris, W. De Ferranti, D. Lucarelli, L. Viola, and M. Biercuk, *Nature communications* **8**, 1 (2017).
- [49] Y. Sung, F. Beaudoin, L. M. Norris, F. Yan, D. K. Kim, J. Y. Qiu, U. von Lüpke, J. L. Yoder, T. P. Orlando, S. Gustavsson, *et al.*, *Nature communications* **10**, 1 (2019).
- [50] V. Frey, L. M. Norris, L. Viola, and M. J. Biercuk, *Phys. Rev. Applied* **14**, 024021 (2020).
- [51] U. von Lüpke, F. Beaudoin, L. M. Norris, Y. Sung, R. Winik, J. Y. Qiu, M. Kjaergaard, D. Kim, J. Yoder, S. Gustavsson, L. Viola, and W. D. Oliver, *PRX Quantum* **1**, 010305 (2020).
- [52] W. I. L. Lawrie, M. Russ, F. van Riggelen, N. W. Hendrickx, S. L. de Snoo, A. Sammak, G. Scappucci, and M. Veldhorst, “Simultaneous driving of semiconductor spin qubits at the fault-tolerant threshold,” (2021).
- [53] L. Cywiński, R. M. Lutchyn, C. P. Nave, and S. Das Sarma, *Phys. Rev. B* **77**, 174509 (2008).
- [54] L. M. Norris, D. Lucarelli, V. M. Frey, S. Mavadia, M. J. Biercuk, and L. Viola, *Phys. Rev. A* **98**, 032315 (2018).
- [55] T. Chalermputitarak, B. Tonekaboni, Y. Wang, L. M. Norris, L. Viola, and G. A. Paz-Silva, *PRX Quantum* **2**, 030315 (2021).
- [56] See supplemental material for further details.
- [57] E. J. Connors, J. Nelson, L. F. Edge, and J. M. Nichol, *Nature communications* **13**, 1 (2022).
- [58] J. He, Q. Liu, Z. Yang, Q. Niu, X. Ban, and J. Wang, *Phys. Rev. A* **104**, 063120 (2021).
- [59] G. Quiroz, P. Titum, P. Lotshaw, P. Lougovski, K. Schultz, E. Dumitrescu, and I. Hen, arXiv:2109.04482 (2021).
- [60] J. Morris, F. A. Pollock, and K. Modi, “Non-markovian memory in ibmqx4,” (2019).
- [61] Y.-Q. Chen, K.-L. Ma, Y.-C. Zheng, J. Allcock, S. Zhang, and C.-Y. Hsieh, *Phys. Rev. Applied* **13**, 034045 (2020).
- [62] G. A. White, C. D. Hill, F. A. Pollock, L. C. Hollenberg, and K. Modi, *Nature Communications* **11**, 1 (2020).
- [63] H. Zhang, B. Pokharel, E. Levenson-Falk, and D. Lidar, *Phys. Rev. Applied* **17**, 054018 (2022).
- [64] A. M. Souza, G. A. Álvarez, and D. Suter, *Phys. Rev. A* **85**, 032306 (2012).
- [65] P. Wocjan, *Phys. Rev. A* **73**, 062317 (2006).
- [66] R. Stine, *Sociological Methods & Research* **18**, 243 (1989), <https://doi.org/10.1177/0049124189018002003>.
- [67] N. Ezzell, B. Pokharel, L. Tewala, G. Quiroz, and D. A. Lidar, arXiv:2207.03670 (2022).
- [68] K. Schultz, G. Quiroz, P. Titum, and B. D. Clader, *Phys. Rev. Research* **3**, 033229 (2021).
- [69] A. Murphy, J. Epstein, G. Quiroz, K. Schultz, L. Tewala, K. McElroy, C. Trout, B. Tien-Street, J. A. Hoffmann, B. D. Clader, J. Long, D. P. Pappas, and T. M. Sweeney, *Phys. Rev. Research* **4**, 013081 (2022).